Field and temperature dependence of intrinsic diamagnetism in graphene: Theory and experiment

Zhilin Li,[1] Lianlian Chen,[1] Sheng Meng,[1,*] Liwei Guo,[1,†] Jiao Huang,[1] Yu Liu,[1] Wenjun Wang,[1] and Xiaolong Chen[1,2,‡]

[1]*Beijing National Laboratory for Condensed Matter Physics, Institute of Physics, Chinese Academy of Sciences, Beijing 100190, China*

[2]*Collaborative Innovation Center of Quantum Matter, Beijing 100190, China*

(Received 31 August 2014; revised manuscript received 14 March 2015; published 27 March 2015)

Intrinsic diamagnetism of graphene is studied both theoretically and experimentally, to unravel the magnetic response of chiral massless fermions. Comprehensive formulas predicting the variation of graphene magnetization with magnetic field and temperature are developed. Graphene magnetization M at low temperatures is particularly large and $M \propto -\sqrt{B}$, intrinsically different from normal materials. The quantum Berry phase of π and linear energy dispersion are responsible for this intriguing macroscopic behavior. The temperature dependence of magnetization is successfully formulated by a Langevin-like function. The de Haas–van Alphen oscillations are predicted in the case of doping. Correspondingly, experiments at different temperatures are conducted on highly pure, mass-produced graphene flakes derived from SiC single crystals, which exhibit very strong diamagnetism. The measured results agree well with the theoretical ones in both magnitude and trend.

DOI: 10.1103/PhysRevB.91.094429 PACS number(s): 73.20.−r, 71.10.−w, 73.22.Pr, 75.20.−g

I. INTRODUCTION

Graphene, possessing an ideal two-dimensional honeycomb lattice, exhibits a number of intriguing properties [1–10] owing to its peculiar linear dispersive band structure that has been well studied since its discovery in 2004. The intrinsic magnetism of this chiral Dirac electron system, however, needs to be studied further in both theoretical and experimental aspects. As graphene is a typical electron system featuring touching bands at the Dirac point, single-band approaches (e.g., Landau-Peierls approach [11,12]) failed to produce the correct susceptibility. Fukuyama and Kubo [13] took the interband effect into consideration and obtained a chemical-potential-dependent diamagnetism. McClure [14] figured out the special Landau levels (LLs) of graphene in a magnetic field, and derived the susceptibility at a high-temperature limit. Sharma [15] took the trigonal wrapping of the Fermi surfaces into account and made a modification to the previous result. The recent work of Koshino *et al.* [16–18] predicts that graphene should have magnetic responses different from graphite and graphene multilayers, mainly due to the different crystal symmetry and interlayer interactions. Raoux *et al.* [19] showed the critical role of the electron Berry phase in graphene's orbital magnetism, and derived the zero-temperature susceptibility. However, a comprehensive relation of magnetization M with magnetic field B and temperature T, essential for any rigorous experimental verification, is still not available.

On the other hand, in the experimental aspect, measurements are often limited by either an insufficient amount or purity of graphene samples. In the former case the response signal is too weak and has a large uncertainty, while para- and ferromagnetism are often observed, which are likely to be due to the 3*d*-metal impurities in measured graphene, as in the latter case. Other experiments are focused on the point defects and zigzag edge related spin ordering of nanoscale graphene [20–23], not belonging to the scope of an intrinsic property of graphene. In this regard, mass-produced, highly pure graphene of good quality is strongly desired.

Here we investigate graphene magnetization both theoretically and experimentally. An explicit form of magnetization M with respect to field B and temperature T is derived from evaluating the grand canonical thermodynamic potential of chiral Dirac electrons. A nonlinear dependence of diamagnetism on field and temperature is observed due to the π Berry phase and the linear dispersion in graphene. Experimental measurements were conducted on mass-produced, high-purity graphene samples derived from the thermal decomposition of SiC crystals, which exhibit strong diamagnetism and can be levitated above NdFeB permanent magnets [see Fig. 1(a)]. The measured magnetization M varies with field B in a similar way as predicted by our theoretical model, and is intrinsically different compared to that of graphite [Fig. 1(c)]. The magnetic susceptibility of graphene is about two orders of magnitude larger than normal materials, and is even two to three times stronger than graphite. These theoretical and experimental results will be helpful in further studies of the magnetism of graphenelike and graphene-related materials.

II. LANDAU LEVELS IN GRAPHENE

We consider low-energy excitations in graphene, i.e., the π electrons near the Dirac point occupying the energy levels between $-E_c$ and E_c, where E_c is the cutoff energy. E_c is smaller than t, the nearest-neighbor hopping energy. In a simplest tight-binding model, the band energy ϵ and the density of states (DOS) $g(\epsilon)$ can be expressed as [2,24]

$$\epsilon = \hbar v_F k, \quad v_F = \frac{3}{2} a_0 t/\hbar. \tag{1}$$

$$g(\epsilon) = \gamma|\epsilon|, \quad \gamma = 2\frac{A}{\pi}\frac{1}{(\hbar v_F)^2}. \tag{2}$$

Here v_F is Fermi velocity, $A = \frac{3\sqrt{3}}{2}a_0^2$ the area of the unit cell, and a_0 the carbon-carbon bond length. By fitting to *ab initio* band structures, we obtain the parameters as follows: $\gamma \approx 0.123$ (eV)$^{-2}$ (unit cell)$^{-1}$, $v_F \approx 7.9 \times 10^5$ m/s, and $t \approx 2.44$ eV. Reference [4] recommends similar parameters.

*smeng@iphy.ac.cn
†lwguo@aphy.iphy.ac.cn
‡chenx29@aphy.iphy.ac.cn

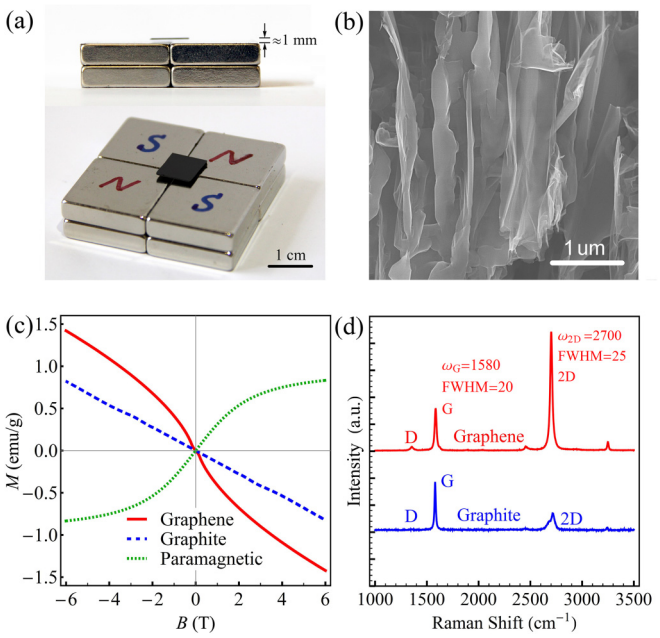

FIG. 1. (Color online) (a) A $10 \times 10 \times 0.3$ mm^3 piece of graphene sample produced from SiC is levitated by 1 mm above NdFeB magnets. (b) The scanning electron microscope (SEM) image of the graphene. (c) The magnetization curve of graphene and graphite ($T = 10$ K), and typical paramagnetic materials (schematic). (d) Raman spectra for graphene and graphite samples. The wavelength of the excitation laser is 532 nm.

When a magnetic field B is applied vertically to the graphene plane, the levels originally ranging from $E(N-1/2)$ to $E(N+1/2)$ now coalesce into the newly formed Nth Landau level $E(N)$ with the degeneracy $D(B)$ [4,14], as shown in Fig. 2. Here

$$E(N,B) = \mathrm{sgn}(N)\sqrt{2e\hbar v_F^2 B|N|}, \tag{3}$$

$$D(B) = \int_{E(N-1/2)}^{E(N+1/2)} \gamma|\epsilon|d\epsilon = \gamma e\hbar v_F^2 B. \tag{4}$$

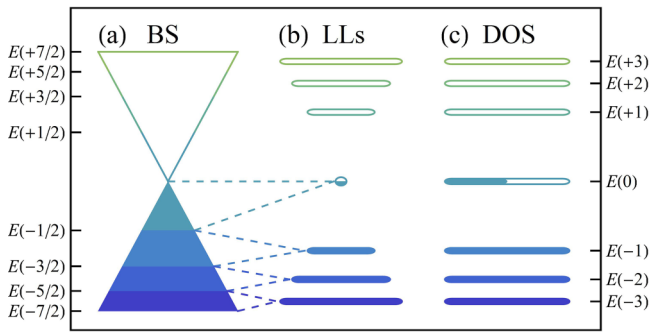

FIG. 2. (Color online) (a) The band structure (BS) of graphene near the Fermi level. Electrons filled the energy levels up to the Dirac point. (b) Unevenly spaced Landau levels (LLs) in magnetic field. The zeroth Landau level is half filled. The dashed lines show how the electrons coalesce into the LLs. (c) The density of states (DOS) of the LLs is in the form of a Dirac comb with uneven energy spacing.

The Landau level number $N = -m \ldots -1, 0, 1 \ldots +m$, where $m = \lfloor \frac{E_c^2}{2e\hbar v_F^2 B} + \frac{1}{2} \rfloor$; $\lfloor x \rfloor$ represents the floor function and gives the greatest integer less than or equal to x.

The Landau levels are unevenly spaced and symmetrically arranged around the zero-energy level at the Dirac point—much different from a conventional two-dimensional electron gas where Landau levels are uniformly spaced with a zero point energy of $\frac{1}{2}\hbar\omega$ [11]. This is the main feature of graphene's LLs, which has been confirmed by its quantum Hall effect [5–8], and is proved to be a direct effect of the electrons' Berry phase of π [1,6,10,25,26]. It should be noted that the $N = 0$ LL is shared between the valence and conduction band, and is half filled for undoped graphene.

III. MAGNETIZATION AT ZERO TEMPERATURE

Since $M = -\frac{\partial F}{\partial B}$, and $F = U - TS$, the entropy S makes no contribution to free energy F at zero temperature $T = 0$. The internal energy in the zero and nonzero field is denoted as U_0 and U_B, respectively. M refers to the magnetic moment per unit cell and $M = -\frac{\partial(U_B - U_0)}{\partial B}$. We have

$$U_0 = \int_{E(-m-1/2)}^{0} \epsilon\gamma|\epsilon|d\epsilon = -\frac{\gamma}{3}\left[2e\hbar v_F^2 B(m+1/2)\right]^{3/2}, \tag{5}$$

$$U_B = E(0)\frac{D(B)}{2} + \sum_{N=-m}^{-1} E(N)D(B). \tag{6}$$

Here m is a very large number (e.g., for $E_c = 1$ eV and $B = 1$ T, $m > 1000$). Using the power series expansion and Euler equation, we have

$$\left(m + \frac{1}{2}\right)^{3/2} \approx m^{3/2} + \frac{3m^{1/2}}{4} + \frac{3m^{-1/2}}{32} - \frac{m^{-3/2}}{128}, \tag{7}$$

$$\sum_{N=1}^{m}\sqrt{N} = H_m^{(-1/2)} \approx \frac{2m^{3/2}}{3} + \frac{m^{1/2}}{2} + \frac{m^{-1/2}}{24} - \frac{\zeta(3/2)}{4\pi}, \tag{8}$$

where $H_m^{(-1/2)}$ represents the mth harmonic number of order $-1/2$. The last term of Eq. (8) is in the form of an Euler-Riemann zeta function, $\frac{\zeta(3/2)}{4\pi} \approx 0.208$.

Hence we obtain that $\Delta U = U_B - U_0 \approx 0.882\frac{\gamma}{3}(e\hbar v_F^2 B)^{3/2}$, and

$$M = -\frac{\partial \Delta U}{\partial B} = -0.882\frac{\gamma}{2}\left(e\hbar v_F^2\right)^{3/2}\sqrt{B}. \tag{9}$$

Here 0.882 is the numerical approximation of the constant $\frac{3\zeta(3/2)}{2\sqrt{2\pi}}$.

The simple relation of $M \propto -\sqrt{B}$ at $T = 0$ suggests an intrinsically nonlinear diamagnetism of graphene, consistent with Ref. [19]. To obtain a better understanding, contributions from each individual LL are analyzed. From Figs. 2(a) and 2(b), it is seen that for electrons on $N \neq 0$ LLs, the energy increase and decrease cancel out almost completely, making these electrons contribute little to the total energy change. Electrons which condense into the $N = 0$ LL, with energy originally ranging from $E(-1/2)$ to 0, provide a net energy

gain, $\Delta U_{N=0} = 0 - \int_{E(-1/2)}^{0} \epsilon\gamma|\epsilon| d\epsilon = \frac{\gamma}{3}(e\hbar v_F^2 B)^{3/2}$. So the magnetization

$$M_{N=0} = -\frac{\partial \Delta U}{\partial B} = -\frac{\gamma}{2}\left(e\hbar v_F^2\right)^{3/2}\sqrt{B}. \quad (10)$$

Comparing Eq. (10) with Eq. (9), the only difference is that the prefactor is now 1 instead of 0.882. This suggests that electrons near the Fermi level which collapse into the zeroth LL make the dominant contribution to graphene diamagnetism, while the electrons in all the other LLs provide a small fraction of paramagnetism.

The existence of the Landau level at $E = 0$ is a result of the Berry phase of π [4,6,26], the very reason for the large diamagnetism of graphene, and the square root relation is a direct consequence of the linear dispersion band structure. Additionally, as the Fermi level is kept at zero, the de Haas–van Alphen oscillations will be substantially suppressed.

IV. MAGNETIZATION AT FINITE TEMPERATURES

For any practical test or application, the $T \neq 0$ case must be investigated. To this end, following Ghosal [27] and co-workers' procedure, we begin with grand canonical ensembles to study the temperature-dependent magnetization. The grand canonical thermodynamic potentials without and with magnetic fields are denoted as Ω_0 and Ω_B, respectively:

$$\Omega_0 = -k_B T \int_{E(-m-\frac{1}{2})}^{E(+m+\frac{1}{2})} \gamma|\epsilon| \ln\left[1 + \exp\left(-\frac{\epsilon - \mu}{k_B T}\right)\right] d\epsilon, \quad (11)$$

$$\Omega_B = -k_B T\, D(B) \sum_{n=-m}^{m} \ln\left[1 + \exp\left(-\frac{E(N) - \mu}{k_B T}\right)\right], \quad (12)$$

$$M = -\frac{\partial(\Omega_B - \Omega_0)}{\partial B}. \quad (13)$$

For undoped graphene, the chemical potential $\mu = 0$. Numerical solutions based on Eqs. (11)–(13) are shown in Figs. 3(a) and 3(c), as a series of markers. To compare with the experimental measurements, M is put in a proper unit of emu/g and multiplied by a factor of 1/2. This factor approximately accounts for the average effect of random orientations of graphene flakes.

For further convenient use, we try to provide an approximate solution in an analytical form. As we have obtained the solution at the low-temperature limit, what we need to do next is to find a temperature-dependent term. The electrons occupy the energy levels, obeying Fermi-Dirac statistics. At the low-field high-temperature limit, the Boltzmann statistic is a good approximation. When they coalesce into one level, the induced magnetization produced by the energy change should be in the form of a Langevin function, just as the magnetization of paramagnetic ions where the electrons on degenerate levels go into several split levels, but with different signs. The uneven space between the Landau levels does not matter in this case, but at a high-field low-temperature limit, the effect resulting from the uneven space between Landau levels cannot be ignored. In this case, an additional modifying

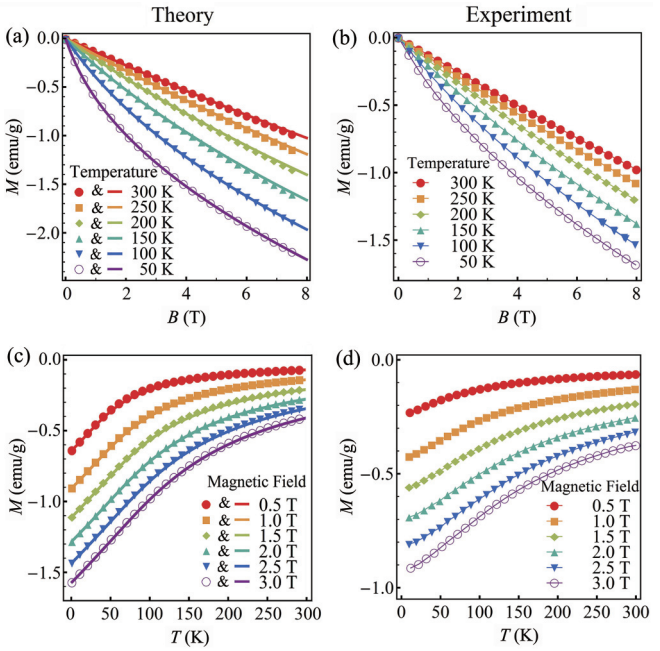

FIG. 3. (Color online) (a) Calculated and (b) measured magnetization M as a function of magnetic field B at different temperatures. (c) Calculated and (d) measured magnetization M as a function of temperature T in different magnetic fields. Note that in the theoretical part [(a) and (c)], the numerical results are plotted as a series of markers, and analytical approximations as continuous lines, while the experimental results [(b) and (d)] are represented by markers joined by lines.

factor is needed to merge the differences. Now, starting from the $T = 0$ cases, we introduce a modified Langevin function to account for the variation in magnetization due to the energy change as influenced by temperature:

$$M = -0.882\frac{\gamma}{2}\left(e\hbar v_F^2\right)^{3/2}\sqrt{B}\,L\left(\frac{\sqrt{e\hbar v_F^2 B\alpha(T)}}{\sqrt{2}k_B T}\right). \quad (14)$$

Here $L(x)$ is the Langevin function defined as $L(x) = \coth(x) - \frac{1}{x}$. $L(x)$ is approximately $x/3$ when x approaches 0, and 1 when x goes to infinity. $\alpha(T) = \frac{C}{C+\sqrt{T}}$ with a variable parameter C gives a slight modification to M. When C is chosen properly (e.g., $C = 45$, in units of $K^{1/2}$), the difference between the analytical and numerical results can be less than 1%. As seen in Figs. 3(a) and 3(c), the differences between the approximate functions (lines) and the numerical results (markers) are negligibly small.

Therefore, in the low-temperature high-field limit, i.e., $E(1) \gg k_B T$, Eq. (14) can be reduced to

$$M \approx -0.882\frac{\gamma}{2}\left(e\hbar v_F^2\right)^{3/2}\sqrt{B} + 0.882\frac{\gamma}{2}e\hbar v_F^2\sqrt{2}k_B T, \quad (15)$$

while in the high-temperature low-field limit, i.e., $E(1) \ll k_B T$, Eq. (14) reduces to the classical form

$$M \approx -0.882\frac{\gamma}{2}\frac{\left(e\hbar v_F^2\right)^2 B}{3\sqrt{2}k_B T}. \quad (16)$$

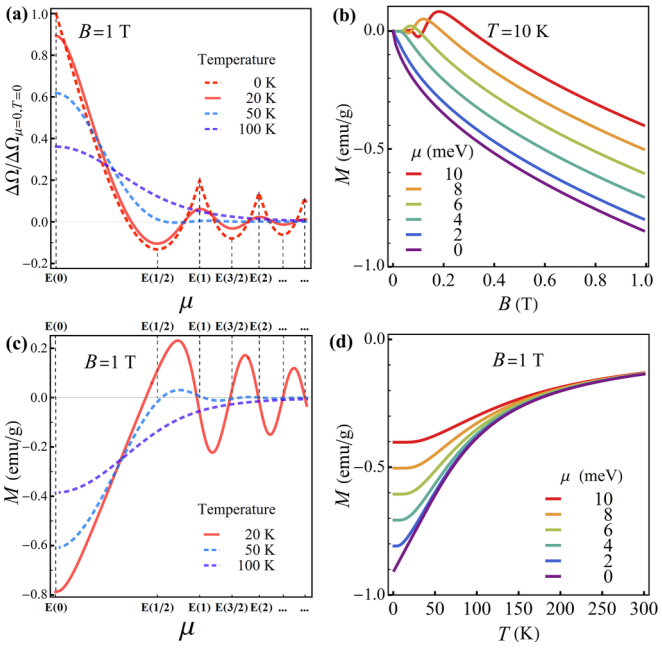

FIG. 4. (Color online) The calculated magnetic properties of doped graphene. (a), (c) Dependence of grand potential and magnetization on the chemical potential at different temperatures. (b), (d) Dependence of magnetization on magnetic field and temperature at different doping levels.

We find that the M-B relation at low temperatures is intrinsically nonlinear, in the form of $M \propto -\sqrt{B}$, while it changes to a linear dependence on B at high temperatures. For a given B, it is seen that at low temperatures $M \propto T + \text{const}$, mainly due to an increasing entropy with increasing T, and at high temperatures $M \propto -1/T$, implying a decreased energy gain due to the more diffuse electron distribution.

V. DOPED CASES

Electron and hole doping will give similar results due to band structure symmetry. For electron doping, $\mu > 0$. When graphene is slightly doped, e.g., $\mu < E(1/2)$, it is straightforward to predict that the diamagnetism will be suppressed due to a canceling out of the energy change of the doping electrons. As seen in Figs. 4(a) and 4(c), temperature will cause a smearing effect on the system and make the curves looks smoother with less obvious oscillations.

The de Haas–van Alphen oscillations will appear as the highest occupied Landau level sweeps through the Fermi surface as B increases [see Fig. 4(b)]. To show more details of the oscillations, we focus on the relatively lower field in the range of 0–1 T. The M-T function for different doping levels is depicted in Fig. 4(d). It is seen that the low-temperature magnetization is more sensitive to the doping, and at the low-temperature limit, the curves tend to be flatter.

VI. EXPERIMENT

To test the validity of the above predictions, we perform experimental measurements on the diamagnetism of graphene.

TABLE I. Impurity concentrations.

Element	Detection limit	Concentration[a]
Fe	5.00×10^{15}	[b]
Co	7.00×10^{15}	
Ni	1.00×10^{16}	
V	1.00×10^{15}	
Mn	2.00×10^{15}	
Ti	5.00×10^{13}	2.61×10^{15}
Cu	5.00×10^{16}	
Al	1.00×10^{14}	
B	1.00×10^{14}	1.96×10^{17}
O	1.00×10^{17}	3.32×10^{18}
Si	1.00×10^{17}	2.57×10^{19}
S	1.00×10^{16}	

[a]In units of atoms/cm^3.
[b]Below or near the detection limit.

This poses a severe challenge. The susceptibility of graphene is in the order of 10^{-5} emu g^{-1} Oe^{-1}, so mass-produced graphene (~10 mg) of high purity (concentrations of 3d-metal impurities <1ppm) is essential.

Graphene samples prepared by chemical vapor deposition (CVD), reduced graphene oxide, or mechanical exfoliation of highly oriented pyrolytic graphite are not suitable, so mass-produced graphene derived from a SiC single crystal is a better choice. A high vacuum (~10^{-4} Pa), high growth temperature (>1500 °C), all-graphite environment (high-purity graphite crucible, induction heated), and a long enough growing time (~8h) are employed to make sure the graphene sample is extremely pure and composed of randomly stacked, weakly coupled layers. More details can be consulted elsewhere in our previous work [28].

The technique of secondary ion mass spectrometry (SIMS) is capable of detecting impurity elements at <0.1ppm (part per million) concentration. For our graphene sample, the detected concentrations of 3d metals (Fe, Co, Ni, V, Mn, Ti, Cu) are less than 1 ppm, and B ~ 0.001%, O ~ 0.01%, Si ~ 0.1%, as seen in Table I. Here the concentration of carbon atoms is 2.0×10^{22} atoms/cm^3.

Figures 1(b) and 1(d) show the scanning electron microscope image and Raman spectrum of our graphene sample derived from a 6H-SiC single crystal, respectively. Graphene sheets of the size of several microns are obtained. The small D peak in the Raman spectrum indicates a good quality of graphene, with few defects and disorders. The sharp and symmetric 2D peak and its high intensity ratio to the G peak (I_{2D}/I_G) suggest the presence of single-layer or few-layer graphene with weak interlayer coupling [29,30]. In addition, the levitation shown in Fig. 1(a) due to the strong diamagnetism of the graphene thus obtained demonstrated that it can meet our demands.

The magnetizations are measured in a physical property measurement system. The $M(B)$ and $M(T)$ curves are shown in Figs. 3(b) and 3(d). They agree well with the theoretical ones in shapes, trends, and main characters. We can see the magnetization and susceptibility reach about -0.5 emu g^{-1} and -1×10^{-5} emu g^{-1} Oe^{-1}, respectively, under a moderate

field (∼4T) at room temperature and are almost doubled at 50 K. The field-dependent magnetism exhibits a nearly linear relation at high temperatures and switches to a square root relation as the temperature decreases, confirming the validity of Eqs. (15) and (16). The predicted values are a little higher than experiments but still acceptable.

Considering that the theoretical results are the largest possible diamagnetism one can get in ideal conditions, the agreement between theory and experiment is quite satisfying. In the theoretical aspect, the Landau level broadening (introduced by temperature and defects) is not accounted for in this model, leading to an overestimation of the diamagnetism. In the experimental aspect, slight doping [14,19] and defect-introduced localized states [31,32] can result in a sharp decrease in diamagnetism. Any possible magnetic impurities, point defects, or zigzag edges in graphene can introduce para- or ferromagnetism, partially canceling out the diamagnetism [20–23].

It should be noted that the $M(B)$ curves of graphene share some similarities to those of type-II superconductors [33]. One may tend to mistakenly assign the observed diamagnetism as evidence of superconductivity. It is strongly recommended that great care be taken when measuring weak magnetic signals and subtracting the diamagnetic background of graphene-related materials.

VII. CONCLUSION

The diamagnetism of graphene is about two orders of magnitude larger than normal materials, and has interesting magnetic field and temperature dependences. The approximate analytical forms of graphene magnetization at both the quantum (low T, strong B) and classical (high T, weak B) regimes are theoretically obtained and experimentally confirmed. The nonlinear field dependence in the former case suggests that graphene diamagnetism is a phenomenon of chiral Dirac electrons and a macroscopic consequence of the π quantum Berry phase. Note the model presented here is not constrained to specific materials, and would be generally applicable to other massless chiral fermion systems.

ACKNOWLEDGMENTS

Z.L.L. would like to thank X. C. Huang, X. Wu, and H. Z. Zhang of the Institute of Physics, CAS, and J. H. Wang of Wuhan University for fruitful discussions. This work was partly supported by the Ministry of Science and Technology of China (Grants No. 2011CB932700 and No. 2013CBA01603), the Chinese Academy of Sciences (Grant No. KJCX2-YW-W22), and the National Natural Science Foundation of China (Grants No. 51272279 and No. 51072223).

[1] A. K. Geim and K. S. Novoselov, Nat. Mater. **6**, 183 (2007).
[2] A. H. Castro Neto, F. Guinea, N. M. R. Peres, K. S. Novoselov, and A. K. Geim, Rev. Mod. Phys. **81**, 109 (2009).
[3] M. Sprinkle, D. Siegel, Y. Hu, J. Hicks, A. Tejeda, A. Taleb-Ibrahimi, P. Le Fèvre, F. Bertran, S. Vizzini, H. Enriquez, S. Chiang, P. Soukiassian, C. Berger, W. A. de Heer, A. Lanzara, and E. H. Conrad, Phys. Rev. Lett. **103**, 226803 (2009).
[4] E. Y. Andrei, G. Li, and X. Du, Rep. Prog. Phys. **75**, 056501 (2012).
[5] K. S. Novoselov, A. K. Geim, S. V. Morozov, D. Jiang, M. I. Katsnelson, I. V. Grigorieva, S. V. Dubonos, and A. A. Firsov, Nature (London) **438**, 197 (2005).
[6] M. O. Goerbig, Rev. Mod. Phys. **83**, 1193 (2011).
[7] K. S. Novoselov, Z. Jiang, Y. Zhang, S. V. Morozov, H. L. Stormer, U. Zeitler, J. C. Maan, G. S. Boebinger, P. Kim, and A. K. Geim, Science **315**, 1379 (2007).
[8] V. P. Gusynin and S. G. Sharapov, Phys. Rev. Lett. **95**, 146801 (2005).
[9] C. L. Kane and E. J. Mele, Phys. Rev. Lett. **95**, 226801 (2005).
[10] K. S. Novoselov, E. McCann, S. V. Morozov, V. I. Fal'ko, M. I. Katsnelson, U. Zeitler, D. Jiang, F. Schedin, and A. K. Geim, Nat. Phys. **2**, 177 (2006).
[11] L. Landau, Z. Phys. **64**, 629 (1930).
[12] R. Peierls, Z. Phys. **80**, 763 (1933).
[13] H. Fukuyama and R. Kubo, J. Phys. Soc. Jpn. **27**, 604 (1969).
[14] J. W. McClure, Phys. Rev. **104**, 666 (1956).
[15] M. P. Sharma, L. G. Johnson, and J. W. McClure, Phys. Rev. B **9**, 2467 (1974).
[16] M. Koshino, Y. Arimura, and T. Ando, Phys. Rev. Lett. **102**, 177203 (2009).
[17] M. Koshino and T. Ando, Phys. Rev. B **76**, 085425 (2007).
[18] M. Koshino, Y. Arimura, and T. Ando, in *International Conference of Computational Methods in Sciences and Engineering 2009: (ICCMSE 2009)*, edited by T. E. Simos and G. Maroulis, AIP Conf. Proc. No. 1504 (AIP, Melville, NY, 2012), p. 291.
[19] A. Raoux, M. Morigi, J.-N. Fuchs, F. Piéchon, and G. Montambaux, Phys. Rev. Lett. **112**, 026402 (2014).
[20] O. V. Yazyev, Rep. Prog. Phys. **73**, 056501 (2010).
[21] T. Enoki, Phys. Scr. **2012**, 014008 (2012).
[22] R. R. Nair, M. Sepioni, I. L. Tsai, O. Lehtinen, J. Keinonen, A. V. Krasheninnikov, T. Thomson, A. K. Geim, and I. V. Grigorieva, Nat. Phys. **8**, 199 (2012).
[23] S. S. Rao, S. N. Jammalamadaka, A. Stesmans, V. V. Moshchalkov, J. v. Tol, D. V. Kosynkin, A. Higginbotham-Duque, and J. M. Tour, Nano Lett. **12**, 1210 (2012).
[24] P. R. Wallace, Phys. Rev. **71**, 622 (1947).
[25] M. V. Berry, Proc. R. Soc. London, Ser. A **392**, 45 (1984).
[26] J. N. Fuchs, F. Piéchon, M. O. Goerbig, and G. Montambaux, Eur. Phys. J. B **77**, 351 (2010).
[27] A. Ghosal, P. Goswami, and S. Chakravarty, Phys. Rev. B **75**, 115123 (2007).
[28] L. Chen, L. Guo, Y. Wu, Y. Jia, Z. Li, and X. Chen, RSC Adv. **3**, 13926 (2013).
[29] A. C. Ferrari, J. C. Meyer, V. Scardaci, C. Casiraghi, M. Lazzeri, F. Mauri, S. Piscanec, D. Jiang, K. S. Novoselov, S. Roth, and A. K. Geim, Phys. Rev. Lett. **97**, 187401 (2006).
[30] L. M. Malard, M. A. Pimenta, G. Dresselhaus, and M. S. Dresselhaus, Phys. Rep. **473**, 51 (2009).
[31] S. Wu, L. Jing, Q. Li, Q. W. Shi, J. Chen, H. Su, X. Wang, and J. Yang, Phys. Rev. B **77**, 195411 (2008).
[32] B. Dóra, Low Temp. Phys. **34**, 801 (2008).
[33] E. H. Brandt, Phys. Rev. B **55**, 14513 (1997).